ORIGINAL ARTICLE

Pyrolysis of cocoa shell and its bioenergy potential: evaluating the kinetic triplet, thermodynamic parameters, and evolved gas analysis using TGA-FTIR

Guilherme Davi Mumbach[1] · José Luiz Francisco Alves[1] · Jean Constantino Gomes da Silva[1] · Michele Di Domenico[2] · Rennio Felix de Sena[3] · Cintia Marangoni[1] · Ricardo Antonio Francisco Machado[1] · Ariovaldo Bolzan[1]

Abstract

This study presents the first attempt to focus on the cocoa shell pyrolysis in terms of kinetic triplet, thermodynamic parameters, and evolved volatile analysis using the TGA-FTIR technique. For reliable interpretation of the multistep pyrolysis of cocoa shell, the multiple kinetic triplets were adequately estimated by a combined kinetic procedure using five independent parallel reactions with the Vyazovkin isoconversional method, the compensation effect, and the master plot method. According to the results, the multiple kinetic triplets were able to describe the pyrolysis behavior of the cocoa shell with an accuracy of $R^2 > 0.9446$ and the pyrolysis mechanisms exhibited different reaction models (n-order and contracting cylinder). Evolved volatile analysis suggested the presence of high-energy compounds (aromatic) and useful chemicals (aldehyde, ketone, esters, ether, and alcohols). The pre-exponential factors for the five pseudo-components of cocoa shell pyrolysis ranged from 2.56×10^{11} to 8.66×10^{16} min^{-1} (derived from the compensation effect method), while the values of E_a ranged from 99 to 271 kJ mol^{-1}. From a comparative analysis, it was found that the results from the compensation effect method ensured the overall kinetic expression to be consistent with the experimental cocoa shell pyrolysis behavior. In contrast, the overall kinetic expression using pre-exponential factors derived from Kissinger's method failed to match the experimental curves. The pyrolytic conversion of cocoa shell into bioenergy appeared as potentially viable ($E_a - \Delta H \leq 5.5$ kJ mol^{-1}). The promising findings on the cocoa shell pyrolysis can expand the use of this residue in bioenergy applications, consisting of a great attempt toward its valorization.

✉ José Luiz Francisco Alves
  zeluiz_alves@hotmail.com; jose.alves@posgrad.ufsc.br

[1] Graduate Program in Chemical Engineering, Department of Chemical Engineering and Food Engineering, Federal University of Santa Catarina, Florianópolis, SC 88040-900, Brazil

[2] Department of Engineering, Federal University of Technology – Paraná (UTFPR), Francisco Beltrão, PR 85601-970, Brazil

[3] Laboratory of Activated Carbon, Department of Chemical Engineering, Federal University of Paraíba, João Pessoa, PB 58033-455, Brazil

1 Introduction

Nowadays, the search for new, appropriate, and carbon-neutral solid fuel, such as lignocellulosic biomass, has increased. This kind of solid fuel has demonstrated high feasibility of bioenergy production, notably when using a lignocellulosic residue. The utilization of residues for bioenergy production do not compete with the arable fields to food production; therefore, these biomasses are interesting for sustainable development of energy generation. According to the Food and Agriculture Organization of the United Nations (FAO), the worldwide cocoa (*Theobroma cacao*) beans production was 5.25 million tons in 2018, with 239.39 thousand tons resulted from the Brazilian market (about 4.56% of the world's production, which corresponds to the sixth largest production)

🖄 Springer

[1]. In parallel, there is an estimation that 21 million tons of potential feedstock for bioenergy were produced in 2018, taking into account that only 20% of the cocoa fruit was raw material (cocoa beans) for producing chocolate and cocoa-derivative foods [2]. In this context, the cocoa shell, which is a lignocellulosic residue, is generated in significant amounts from cocoa processing (as in the chocolate industry), representing a critical environmental issue for cocoa-producing countries [2]. Bioenergy production from this unexplored lignocellulosic by-product emerges as a potential way to reach zero waste in the chocolate industry. The bioenergy conversion of a lignocellulosic residue by thermochemical routes, when well established, can substantially reduce environmental pollution linked to the sustainable perspective of produce bioenergy products and to diversify the energy matrix with renewable sources.

Among the thermal conversion routes, pyrolysis is an attractive thermochemical technology where the biomass can be potentially converted into different kinds of bioenergy products (pyrolytic syngas, biochar, and bio-oil). The understanding of pyrolysis kinetics, thermodynamics, and evolved gas aspects is indispensable to perform an adequate bioenergy production from the cocoa shell pyrolysis. Thermogravimetric analysis (TGA) coupled with Fourier-transform infrared spectroscopy (FTIR) has become a remarkable tool to monitor the evolved gases produced during the pyrolysis of biomass [3]. Thermogravimetry is a technique often used to evaluate pyrolysis characteristics, such as thermal behavior, kinetic parameters, and thermodynamics parameters. The thermodynamic analysis is often recognized as an extension to kinetic valuation, and it is required to get an insight into the pyrolysis process in terms of energy requirements, which in turn is important in the design of a pyrolysis reactor at the large-scale process, as emphasized by previously published studies [4–6]. From the thermogravimetry data, it is possible to evaluate the kinetic parameters using different mathematical approaches.

Isoconversional (model-free) methods allow the estimation of apparent activation energy (E_a) without making any assumption about the reaction model ($f(\alpha)$)) and pre-exponential factor (A). This assumption is not possible from model fitting because this method is dependent on the reaction model and each experimental condition has a kinetic triplet (E_a, A, and $f(\alpha)$) value [7]. Also, the kinetic triplet estimated from the model-fitting approach shows the disadvantage of being only applicable to the experimental conditions established for the kinetic triplet calculation; thus, these parameters cannot be applied widely [8]. The reaction model during the pyrolysis of biomass can be described by different types of heterogeneous reaction models, such as the nucleation models, reaction order models, geometrical contraction models, and diffusion models, which can be determined by the master plot. For the pre-exponential factor, methods such as the compensation effect and ASTM E698-18 are reported in

the literature; however, the compensation effect has appeared more appropriate for the kinetic study than ASTM E698-18, since the compensation effect takes into account the several reaction models for the determination of A [3, 8–10]. Thus, the kinetic triplet can be adequately extracted from nonisothermal thermogravimetric data by using model-free (isoconversional) methods, the compensation effect method, and the master plot method, which are reliable mathematical methods recommended by the Kinetics Committee of the International Confederation for Thermal Analysis and Calorimetry (ICTAC) [3, 10, 11]. From an engineering perspective, knowledge of the kinetic triplet can be used in computational fluid dynamics (CFD) modeling to support the developing and scaling up of pyrolysis reactors [12–14].

The Vyazovkin method is an advanced isoconversional method that provides E_a as a function of the degree of conversion (α) by nonisothermal conditions with high data accuracy. This method is scarcely explored and reported in the literature [11, 15, 16]. The use of this method requires preliminary data treatment since the biomass pyrolysis involves very complex devolatilization reactions that often incorporate multistep mechanisms, i.e., successive and parallel reactions [17, 18]. In this respect, mathematical tools such as deconvolution fitting functions can extract the several parallel reactions of biomass pyrolysis and provide accurate values of the kinetic triplet [15]. Among the different deconvolution fitting functions found in literature, the Gaussian multi-peak fitting function has proven to be an effective method to extract the single reactions associated with lignocellulosic pseudo-components [3, 19]. The description of each reaction in biomass pyrolysis, reached from deconvolution, can be used in the Vyazovkin isoconversional method to provide suitable kinetic data for biomass pyrolysis. According to Wang et al. [20], few studies report the pyrolytic kinetics of lignocellulosic biomass using a combined kinetic approach.

To the best of our knowledge, there is no literature report about the kinetic triplet, thermodynamic parameters, and evolved gas analysis for cocoa shell pyrolysis to extract essential insights for the future design of effective pyrolysis reactor. Because of this, the novelty of the current study is to present a combined kinetic procedure for interpretation of the multistep process of the cocoa shell pyrolysis in terms of kinetic triplet and thermodynamic parameters. This combined approach is rarely considered for thermochemical conversion since a significant part of published kinetic studies use simplified methods, which accounts for a single-step process because these simplified methods do not provide sufficiently reliable data. This study attempts to estimate pyrolysis characteristics of the cocoa shell, including kinetic triplet, thermodynamic parameters, and evolved gas analysis using a thermogravimetric analyzer coupled with a Fourier-transform infrared spectrometer (TGA-FTIR). The parallel reactions in the cocoa shell pyrolysis were extracted by the deconvolution method

using the symmetrical Gaussian function, where five independent parallel reactions were identified. The kinetic triplet of the corresponding five pseudo-components was separately estimated by using the Vyazovkin method, compensation effect, and master plot method. The applicability of the calculated kinetic triplets was evaluated from the reconstruction of the curves and comparison with the experimental data. Additionally, the compensation effect method and ASTM E698-18 standard (based on the Kissinger's method) were compared in order to indicate the most reliable and accurate method in predicting the pre-exponential factors for the cocoa shell pyrolysis under a multi-component approach. Thermodynamic parameters were calculated with the Eyring theory to discuss the nature of the cocoa shell pyrolysis. The TGA-FTIR technique was used to characterize the volatile products from pyrolysis. It is expected that this study can successfully contribute to future effective bioenergy exploitation from the cocoa shell.

2 Materials and methods

2.1 Preparing and characterizing the cocoa shell

The cocoa shell was reclaimed from a cocoa processing industry located in the state of Bahia (Northeast Brazil). The sample was first washed to remove physical impurities (sand, dust, and mud) and then oven-dried overnight at 378 K. The dried cocoa shell was grounded in a cutting mill (Solab, SL-31, Piracicaba, Brazil) and sieved to obtain a particle size smaller than 150 μm using a mechanical sieve shaker (Bertel, São Paulo, Brazil). The choice for small particle size (< 150 μm) is often indicated for thermogravimetric experiments to reduce heat and mass transfer limitations, as observed in previous studies [5, 21]. The cocoa shell sample (with particle size below 150 μm) was kept in a tightly closed plastic container until the characterization and pyrolysis experiments.

The physicochemical characteristics of the cocoa shell were investigated by proximate analysis, ultimate analysis, heating values, bulk density, and biochemical composition. Proximate analysis was conducted in a thermogravimetric analyzer TGA-Q50 (TA Instruments, New Castle, USA) according to ASTM E1131-08 standard to identify the contents of inherent moisture, volatile matter, fixed carbon, and ash [22]. The contents of carbon, hydrogen, and nitrogen were determined with an Elemental Analyzer 2400 CHN Series II (Perkin-Elmer, Shelton, USA) following the ASTM D5373-08 standard procedure [23]. The content of sulfur was identified by an inductively coupled plasma optical emission spectroscopy analyzer (ICP-OES, Spectro Arcos, Mahwah, USA) according to the ASTM D4239-17 [24], while the content of oxygen was calculated by the difference. The biochemical composition is defined in terms of extractives, hemicellulose, cellulose, and lignin. The weight percentages of these components were experimentally determined according to the Van Soest procedures [25]. Extractives' content was indirectly determined by subtracting the weight percentages of hemicellulose, cellulose, lignin, and ash, from 100 wt% [26]. The higher heating value (HHV) was determined experimentally through an adiabatic bomb calorimeter IKA C200 (IKA Calorimeters, Wilmington, USA) following the ASTM D5865 standard [27]. The lower heating value (LHV) was calculated from the HHV by deducting the latent heat required to vaporize water (LHV(MJ kg^{-1}) = HHV(MJ kg^{-1})-0.2183H(wt%)) [26]. The bulk density was determined by a graduated cylinder using ASTM E873-82 [28].

2.2 Thermogravimetric analysis

Thermogravimetric curves are an appropriate way to estimate the devolatilization kinetics and evaluate the cocoa shell pyrolysis. A thermogravimetric analyzer (STA 449 F3 Jupiter, Netzsch, Germany) was applied to record the mass loss as a function of temperature (nonisothermal measurements) during the pyrolysis of the cocoa shell. The cocoa shell sample (about 10.00 mg with particle size below 150 μm) was placed in an alumina crucible and heated from room temperature to 1100 K at four different heating rates (5, 10, 20, and 30 K min^{-1}) with high-purity nitrogen (99.997%) flowing at 60 mL min^{-1}. Particle size and mass of the cocoa shell sample were kept small to ensure the kinetically controlled regime during devolatilization. These variables agree with previous observations, which indicate that the use of small particle size at low heating rates in thermogravimetric experiments can eliminate heat transfer and intra-particle diffusion limitations [5, 21]. The thermogravimetric data were corrected for the effect of buoyancy by performing a blank experiment for each heating rate condition. The experiments for each condition were performed thrice to confirm the reproducibility of the results and data used for kinetics evaluation.

2.3 Kinetic study

Thermal decomposition kinetics is generally based on a heterogeneous conversion process (solid particle turns into volatiles), which can be mathematically (Eq. 1) expressed by the fundamental solid-volatiles conversion equation associated to Arrhenius equation [10]. The biomass decomposition process occurs in a complex way, where its thermal stability can depend on the distribution of several natural polymers. However, the use of Eq. 1 considers the thermal behavior of a single component, i.e., only the decomposition of one component can be described. Therefore, this equation is not suitable for all kinds of biomasses due to their complex composition, as observed by da Silva [11]. In this context, recent studies are performing the kinetic

evaluation from several single components, being the sum of the thermal effect of each component accounted during the pyrolysis of biomass [3, 8, 15].

The deconvolution algorithm used in this study was designed based on newly published studies about multistep kinetic evaluation for biomass pyrolysis [3, 8]. For this, the overlapped differential kinetic curves derived from TGA data were deconvoluted into multiple pseudo-components associated with contributions of extractives, hemicellulose, cellulose, and lignin, by using the Gaussian multi-peak fitting function. This mathematical function has been successfully employed in dealing with lignocellulosic biomass pyrolysis [3, 19], which often exhibits a pyrolytic behavior with multistep kinetics. For this study, the pseudo-component peaks were extracted using the Microsoft Excel® software and Gaussian function. Thus, the solid-volatiles conversion equation considering the sum of the parallel decomposition reactions of several single components from biomass can be expressed by the right side of Eq. 1:

$$\left(\frac{d\alpha}{dt}\right)_{Biomass} \tag{1}$$

$$= A_{biomass}e^{Ea_{Biomass}/RT}f(\alpha)_{Biomass} \equiv \sum_{i=1}^{N} c_i\left(\frac{d\alpha}{dt}\right)_i = \sum_{i=1}^{N} c_iA_ie^{Ea_i/RT}f(\alpha)_i$$

where α is the conversion, t (min) is the time, A (min^{-1}) is the pre-exponential factor, E_a (kJ mol^{-1}) is the apparent activation energy, T (K) is the temperature, R (kJ mol^{-1} K^{-1}) is the gas constant, $f(\alpha)$ is the reaction model, c is the contributed fraction, the subscript i represents each possible component during the biomass pyrolysis, and N is the total number of components in the biomass. The use of nonisothermal programming at different heating rates (β, K min^{-1}) makes Eq. 1 not widely used for the kinetic study of biomass. Thus, the heating rate (dT/d$t = \beta$) is commonly used in Eq. 1 to provide a more suitable expression (Eq. 2) for the kinetic evaluation under nonisothermal programming:

$$\left(\frac{d\alpha}{dT}\right)_i = \frac{A_i}{\beta}e^{-Ea_i/RT}f(\alpha)_i \tag{2}$$

The E_a values of biomass pyrolysis can be calculated using the differential or integral form of Eq. 2. According to Vyazovkin et al. [10], the differential form provides low accuracy and a high level of noise, scattering the resulting derivative curves, which is not suitable for the determination of E_a values. Thus, the integral form becomes more frequently used for E_a determination. The following equation expresses the integral form of Eq. 2:

$$g(\alpha)_i = \int_0^1 \frac{d\alpha}{f(\alpha)_i} = \frac{A_i}{\beta}\int_{T_0}^{T} e^{-Ea_i/RT}dT \equiv \frac{A_i}{\beta}I(E_{ai}, T) = \frac{A_iE_{ai}}{R\beta}p(x) \tag{3}$$

In Eq. 3, $g(\alpha)$ is the integral form of the reaction model, $I(E_{ai}, T)$ represents the temperature integral inside $g(\alpha)$, and $p(x)$ is the approximation equation for the integral temperature equation with $x = E_a/RT$.

2.3.1 Determination of apparent activation energy

For E_a determination, Eq. 3 has no analytical solution, which becomes necessary to use alternative solution equations, known as approximate equations. Several approximate expressions have been proposed, with most of them proposing a linear relationship of the experimental data, which leads to reduced data accuracy due to various approximations [10]. Thus, according to Vyazovkin et al. [10], the use of numerical integration methods, such as the Vyazovkin method (Eq. 4), can increase the accuracy of the data:

$$\sum_{i=1}^{n}\sum_{j\neq i}^{n} \frac{I(E_a, T_i)\beta_j}{I(E_a, T_j)\beta_i} = n(n-1) \tag{4}$$

where n is the number of experimental runs under different heating rates. In Eq. 4, the E_a is estimated by minimizing the difference between the left-hand and right-hand sides. Thus, E_a values are randomly added until obtaining a minimum value for equality between both sides, where the left side is solved by the approximation method of Senum and Yang fourth [3].

2.3.2 Determination of pre-exponential factor (A)

The compensation effect (Eq. 5), generally used for the estimation of A, is based on the linear relationship between E_a and ln(A). Initially, the compensation parameters (a and b) are obtained from a model fitting at a single heating rate and several reaction models found in the literature [3]. This plotting provides a straight line, where the slope and y-intercept are the compensation parameters a and b, respectively. After finding the compensation parameters, the values of A are estimated with Eq. 5 by adding the E_a values previously determined by an isoconversional method.

$$\ln(A) = aE_a + b \tag{5}$$

The use of compensation effect for A determination is in accordance with ICTAC Kinetics Committee recommendations [10]. The pre-exponential factor can also be obtained by Eq. 6, which is presented by the ASTM E698-18 standard [9]. Equation 6 is based on Kissinger's method (Eq. 7), which is a model fitting. Equation 6 is obtained by rearranging Eq. 7, where the reaction model is assumed as a first-order reaction ($g(\alpha) = -1$):

$$A_i = \frac{\beta E_{a,i}}{RT_{m,i}^2}e^{E_{a,i}/RT_{m,i}} \tag{6}$$

$$\ln\left(\frac{\beta}{T_{m,i}^2}\right) = \ln\left(-\frac{A_iR}{E_{a,i}}g(\alpha)\right) - \frac{E_{a,i}}{RT_{m,i}} \tag{7}$$

In Eq. 6 and Eq. 7, T_m represents the maximum peak temperature (K) observed from the differential thermogravimetric curve (DTG) and the subscript i represents each possible component during the biomass pyrolysis.

2.3.3 Identifying the most probable reaction model ($f(\alpha)$)

The master plot is a well-established mathematical procedure used to determine the most probable reaction model during the pyrolysis of biomass and is based on the comparison between theoretical ($g(\alpha)/g(0.5)$) and experimental curves plotted as $g(\alpha)/g(0.5)$ versus α. The theoretical curves are drawn based on different reaction models found in the literature (Supplementary Table S1), while the experimental curves are obtained from Eq. 8 [3]:

$$\frac{g(\alpha)}{g(0.5)} = \frac{p(x)}{p(x_{0.5})} \tag{8}$$

where $g(0.5)$ is the integral form of the reaction model when the conversion reaches 50% and $p(x_{0.5})$ is the approximate equation when $x = E_a/RT_{0.5}$.

2.3.4 Reconstructing experimental pyrolysis behavior using kinetic triplet

Pyrolysis behavior for each heating rate was mathematically expressed using the kinetic triplet previously determined by isoconversional methods, compensation effect, and master plot. Thus, it plotted the simulated curves in terms of $d\alpha/dt$ versus T to compare with experimental curves and to confirm the obtained kinetic triplet. The simulated curves were solved numerically using the method of fourth-order Runge-Kutta in the pyrolysis kinetic expression, and the results were compared with the experimental curves by the residual (Eq. 9), mean residual (Eq. 10), residual sum of squares (Eq. 11), the total sum of squares (Eq. 12), coefficient of determination (Eq. 13), Chi-square (Eq. 14), and quality of fit (Eq. 15):

$$\text{Residual} = \left(\frac{d\alpha}{dt}\right)_{\exp} - \left(\frac{d\alpha}{dt}\right)_{\text{sim}} \tag{9}$$

$$\text{Mean Residual} = \left[\left(\frac{d\alpha}{dt}\right)_{\exp} - \left(\frac{d\alpha}{dt}\right)_{\text{sim}}\right]/N \tag{10}$$

$$RSS = \sum\left[\left(\frac{d\alpha}{dt}\right)_{\exp} - \left(\frac{d\alpha}{dt}\right)_{\text{sim}}\right]^2 \tag{11}$$

$$TSS = \sum\left[\left(\frac{d\alpha}{dt}\right)_{\exp} - \left(\frac{d\alpha}{dt}\right)_{\text{average}}\right]^2 \tag{12}$$

$$R^2 = 1 - \frac{\sum\left[\left(\frac{d\alpha}{dt}\right)_{\exp} - \left(\frac{d\alpha}{dt}\right)_{\text{sim}}\right]^2}{\sum\left[\left(\frac{d\alpha}{dt}\right)_{\exp} - \left(\frac{d\alpha}{dt}\right)_{\text{average}}\right]^2} \tag{13}$$

$$\chi^2 = \left[\sum\left(\left(\frac{d\alpha}{dt}\right)_{\exp} - \left(\frac{d\alpha}{dt}\right)_{\text{sim}}\right)^2\right]/(N-1) \tag{14}$$

$$QOF(\%) = 100\left\{1 - \left[\sqrt{\sum\left(\left(\frac{d\alpha}{dt}\right)_{\exp} - \left(\frac{d\alpha}{dt}\right)_{\text{sim}}\right)^2/N}\right]/\left(\frac{d\alpha}{dt}\right)_{\max}\right\} \tag{15}$$

In Eq. 9 and Eq. 10, $(d\alpha/dt)_{\exp}$ is the experimental values of $d\alpha/dt$, $(d\alpha/dt)_{\text{average}}$ is the average of experimental values of $d\alpha/dt$, $(d\alpha/dt)_{\text{sim}}$ is the values of $d\alpha/dt$ calculated by the numerical method of fourth-order Runge-Kutta, and N is the number of experimental data points.

2.4 Calculating the thermodynamic functions

The definition of the thermodynamic functions (changes of enthalpy, ΔH; Gibbs free energy, ΔG; and entropy, ΔS) is a precondition to bringing a pyrolysis process to industrial-scale implementation concerning accomplish energy calculations [16]. The thermodynamic calculations regarding the conversion degree were performed using kinetic data (E_a and A) and thermogravimetric data points, from the following equations based on the activated complex theory [29]:

$$\Delta G = E_a + RT_m\ln\left(\frac{k_B T}{hA}\right) \tag{16}$$

$$\Delta H = E_a - RT \tag{17}$$

$$\Delta S = \frac{\Delta H - \Delta G}{T} \tag{18}$$

where k_B represents the Boltzmann constant (1.381×10^{-23} J K^{-1}), h represents the plank constant (6.626×10^{-34} J s^{-1}), and T represents the temperature (K).

2.5 Evolved volatile analysis (TGA-FTIR)

Evolved gas analysis of the pyrolysis of the cocoa shell was performed using a thermogravimetric analyzer (STA 449 F3 Jupiter, Netzsch, Germany) coupled to a Fourier-transform infrared spectrometer (Tensor II, Bruker, Germany). TGA and FTIR devices were connected by a heated line at 503 K, to avoid the condensation of volatile compounds from pyrolysis. A sample mass of 40 mg (with particle size below 150 μm) was heated from room temperature to 1100 K at a heating rate of 20 K min^{-1} under a gas flow rate of 40 mL min^{-1} under a high-purity N_2 atmosphere (99.999%). FTIR spectra of the gaseous products were recorded continuously every 16 s in the spectral region from 4000 to 650 cm^{-1}. The NIST Chemistry

WebBook (https://webbook.nist.gov) was used to identify the components of the evolved gas.

3 Results and discussion

3.1 Physicochemical properties of cocoa shell

According to proximate composition extracted from Fig. 1, the cocoa shell sample presents a volatile matter content of 70.89 wt% and a fixed carbon content of 22.34 wt%, which are comparable with reference fuels such as wood chips and some coals [30]. A high volatile matter implies a high reactivity in comparison with coals. The ash content of 6.77 wt% in the cocoa shell (refer to Table 1) is in accordance with the typical composition of commercial biomass fuels (with a range from 0.6 to 9.8 wt%) [31] and is considerably lower than that of typical Brazilian coals (from 27.4 to 83.1 wt%) [32], which is an advantage for use in the thermochemical route. A low ash content implies a little possibility of incidence of operational problems that can limit mass and heat transfer, mainly at large-scale production, such as fouling and slagging [6]. The measured moisture content of the collected cocoa shell was less than 10 wt%, which is generally regarded as acceptable for biomass thermal conversion [31].

As observed in Table 1, the cocoa shell consists predominantly of carbon (42.16 wt%), hydrogen (6.08 wt%), and oxygen (43.66 wt%). In addition, the low levels of nitrogen (1.32 wt%) and sulfur (0.01 wt%) are favorable for the pyrolytic conversion of the cocoa shell into bioenergy products in an environmentally friendly way, i.e., without significant release of toxic emissions, such as nitrogen oxides (NO_x) and sulfur oxides (SO_x). Note that the elemental composition of several bioresidues suggested as feedstocks for pyrolysis ranges from 41.2 to 49.0 wt% of carbon, from 5.3 to 6.2 wt% of hydrogen,

Table 1 Physicochemical characterization of the cocoa shell, including proximate analysis, ultimate analysis, heating values, bulk density, and biochemical composition

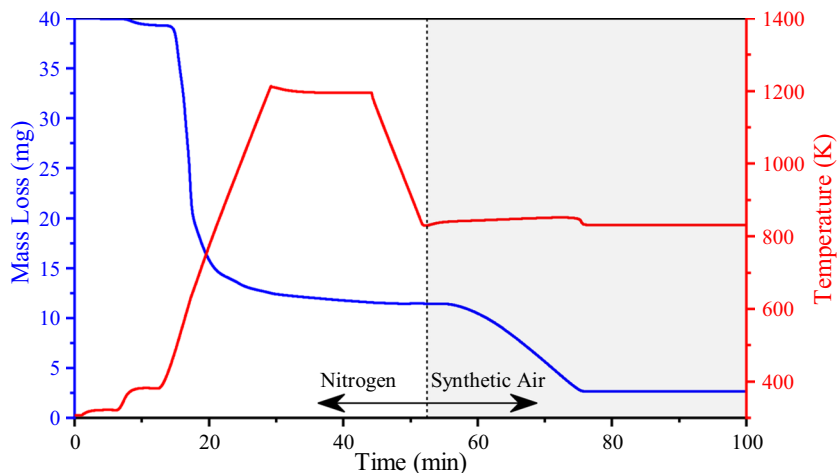|	Cocoa shell
Proximate analysis (wt%)	
Moisture	1.61[a]
Volatile matter	70.89[b]
Fixed carbon	22.34[b,c]
Ash	6.77[b]
Ultimate analysis (wt%)	
Carbon	42.16[b]
Hydrogen	6.08[b]
Nitrogen	1.32[b]
Sulfur	0.01[b]
Oxygen	43.66[b,c]
Heating values (MJ kg^{-1})	
HHV	17.21[b]
LHV	15.97[b]
Bulk density (kg·m^{-3})	581.25[b]
Biochemical composition (wt%)	
Hemicellulose	21.82[d]
Cellulose	30.72[d]
Lignin	31.70[d]
Extractives	15.86[c,d]

[a] Air dried basis
[b] Dry basis
[c] Calculated by difference
[d] Dry ash-free basis

from 41.7 to 46.3 wt% of oxygen, and from 0.4 to 8.2 wt% of nitrogen [33]. The elemental composition of the cocoa shell was shown to be within these ranges of values, which is a favorable indication of its suitability for pyrolytic conversion.

Fig. 1 Thermogravimetric analysis curve for proximate analysis of the cocoa shell

As can be observed in Table 1, the studied cocoa shell sample contains 15.86 wt% of extractives, 21.82 wt% of hemicellulose, 30.72 wt% of cellulose, and 31.70 wt% of lignin (on a dry ash-free basis). Titiloye et al. [34] reported the following biochemical composition (on a dry ash-free basis) for cocoa shell: 23.66 wt% of extractives, 11.97 wt% of hemicellulose, 30.41 wt% of cellulose, and 33.96 wt% of lignin. Thus, for the sample used in this study, the weight fractions of cellulose and lignin are reasonably close to the literature mentioned above. Particularly, the content of hemicellulose agreed very well with the content found for other lignocellulosic residues (18.8–21.5 wt%, on a dry ash-free basis) [5]. Regarding the lignin content, when compared with common agroindustrial residues [33], the value achieved for the cocoa shell is relatively high. This high value is often appropriate for thermochemical conversion processes.

The HHV for the cocoa shell (17.21 MJ kg^{-1}) was higher than that of common samples of lignite coal (13.34 MJ kg^{-1}) [35] and sub-bituminous coal (10.29 MJ kg^{-1}) [32]. Cocoa shell is characterized by its high bulk density (581.25 kg m^{-3}) as compared with other bioenergy feedstock, including wood (500.00 kg m^{-3}), pine (285.00 kg m^{-3}), hazelnut husk (481.00 kg m^{-3}), or palm leaf (298.00 kg m^{-3}) [36]. Usually, a high bulk density value implies a low cost for storage, transportation, and handling. These physicochemical features

illustrate that the cocoa shell can be an eco-friendly and competitive feedstock for bioenergy.

3.2 Pyrolysis characteristics of the cocoa shell

Figure 2a and b show respectively the TGA and DTG curves for the pyrolysis of the cocoa shell as a function of the temperature at four heating rates of 5, 10, 20, and 30 K min^{-1}. The pyrolysis profile (TGA/DTG) of the cocoa shell is qualitatively similar to that reported by Biagini et al. [37]. Five events involving mass loss can be distinguished during the pyrolysis of the cocoa shell, where this complex devolatilization is composed of overlapping events of extractives, hemicellulose, cellulose, and lignin in a parallel decomposition reaction. The first event between 310 and 424 K is the evaporation of inherent moisture with an average mass loss of 3.06 ± 0.19%. The second event, between 400 and 524 K, is possibly the devolatilization of extractives with an average mass loss of 11.73 ± 1.04%. At this temperature range, the devolatilization of extractive species is expected, since they are less thermally stable than hemicellulose, cellulose, and lignin [37, 38]. The third event can be attributed to the devolatilization of hemicellulose between 482 and 579 K, with an average mass loss of 15.09 ± 0.80%. Hemicellulose is composed of various polysaccharides such as xylose, mannose, glucose, and
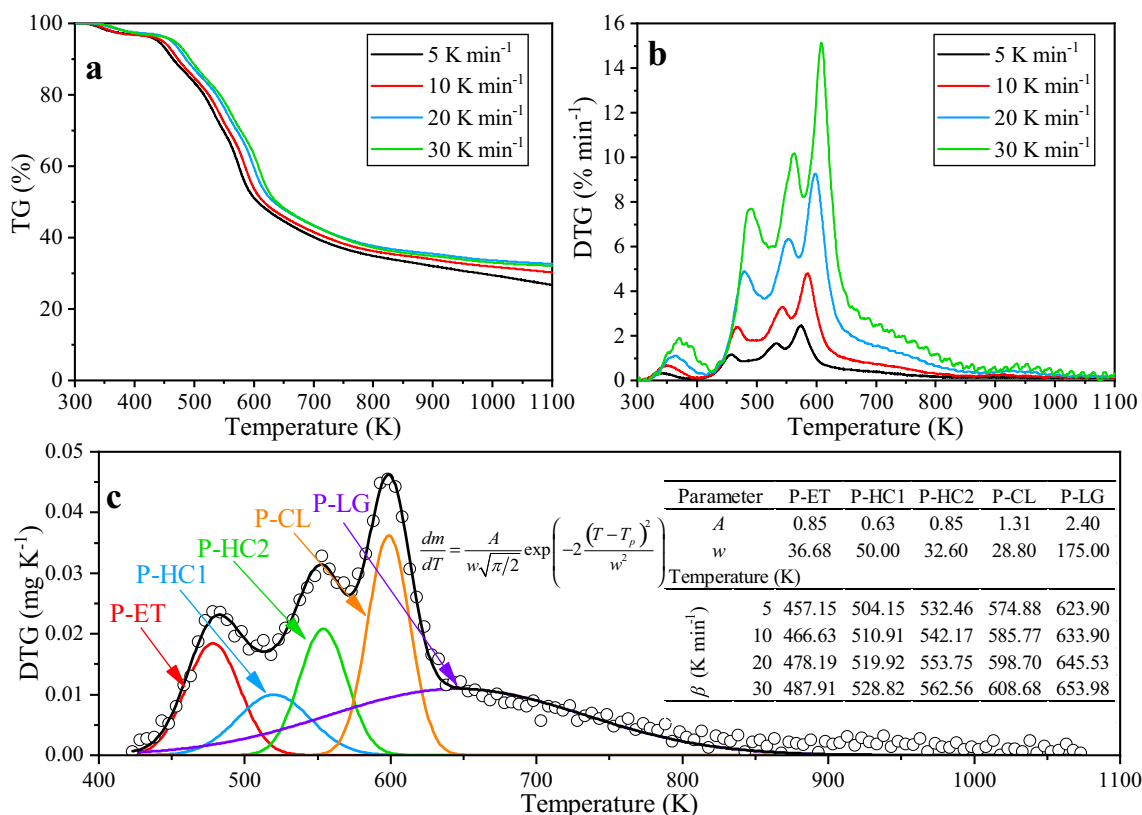
Fig. 2 The nonisothermal **a** TGA and **b** DTG curves for the cocoa shell devolatilization and **c** deconvoluted peaks using Gaussian function and their respective parameters for each independent pseudo-component of cocoa shell devolatilization (at four heating rates)

galactose, and it is decomposed to volatile at low temperatures as compared with cellulose [38]. The fourth event (with an average mass loss of $22.61 \pm 0.30\%$) is characterized by a dominant peak in the DTG profile at a temperature range of 570–600 K, and it is related to cellulose devolatilization [37, 39]. The fifth event (at a temperature range of 616–900 K and with an average mass loss of $13.46 \pm 1.55\%$) is associated with the decomposition of lignin, which often occurs at a large temperature range and slows the decomposition rate. According to Wang et al. [20], this behavior for lignin is observed at a temperature range from 450 to 1170 K.

According to the pyrolysis profiles, the active zone of the cocoa shell pyrolysis occurred within the temperature range of 400–900 K with a characteristic high release of volatile matter (about 62.88%) caused by parallel devolatilization of the pseudo-components (extractives, hemicelluloses, cellulose, and lignin). From the DTG curves, it is clearly observed that cocoa shell pyrolysis is kinetically complex, with multiple overleaped reactions occurring simultaneously. To differentiate the decompositions of hemicellulose, cellulose, and lignin in the active pyrolysis zone, the deconvolution technique was applied to find each independent pyrolytic reaction.

As shown in Fig. 2c, the complex devolatilization behavior of the cocoa shell was deconvoluted into five peaks using the symmetrical Gaussian function, which showed a coefficient of determination (R^2) higher than 0.9837 for the active pyrolysis zone. Contributions of five independent components described the complex pyrolysis behavior of the cocoa shell, referred to as pseudo-extractives (single peak: P-ET), pseudo-hemicelluloses (two peaks: P-HC1 and P-HC2), pseudo-cellulose (single peak: P-CL), and lignin (single peak: P-LG). The assumption of two pseudo-components for hemicellulose (P-HC1 and P-HC2) appears highly applicable since the biomass is composed of different structures and amounts of hemicelluloses (a mixture of polysaccharides), which result in complex thermal behavior. A similar finding was previously reported for wood pyrolysis, with two distinguishable peaks found during the devolatilization of hemicellulose [40].

3.3 Kinetic triplet examination

3.3.1 Estimation of apparent activation energy by Vyazovkin method

Table 2 presents the results of apparent activation energy (E_a) as a function of the degree of conversion (α) calculated by Vyazovkin method for each independent pseudo-component. In this study, the devolatilization of the cocoa shell was considered by the effect of the sum of five different pseudo-components: P-ET, P-HC1, P-HC2, P-CL, and P-LG.

According to Table 2, the relative errors (ε) for all pseudo-component are lower than 1.42%, indicating high accuracy in

the kinetic data obtained by the Vyazovkin method. The first pseudo-component (P-ET) shows a small increase in the E_a value (100.57 to 112.60 kJ mol^{-1}), which was nearly constant at all conversion range. The behavior in E_a values for P-ET indicates the predominance of a single reaction mechanism that describes the P-ET decomposition. In addition, the low E_a values for P-ET indicate low thermal stability, which requires low temperature for complete thermal decomposition. For pseudo-components associated with hemicellulose (P-HC1 and P-HC2), a similar behavior of E_a values during pyrolysis is observed, with a more significant increase of E_a values than that obtained for P-ET. The increase of E_a values for P-HC1 represented 28.67% with a difference of 38.34 kJ mol^{-1} between the initial and final values (133.71 to 172.05 kJ mol^{-1}). Meanwhile, the P-HC2 showed an increase of 21.96 kJ mol^{-1} between the initial and final E_a values (128.63 to 150.59 kJ mol^{-1}), which represented 17.07%. The average value of E_a for P-HC1 was higher than that obtained for P-HC2, thus indicating the high thermal stability of P-HC1 when compared with P-HC2. The thermal stability of P-HC1 can be associated with a low decomposition rate at a wide range of temperatures compared with P-HC2, which results in greater energy required to break chemical bonds. Table 3 presents a comparison between the E_a values for the five pseudo-components of cocoa shell pyrolysis and literature values for the pyrolysis of different types of biomass.

As can be observed in Table 3, the average values of E_a for P-HC1 (152.41 ± 9.88 kJ mol^{-1}) and P-HC2 (139.48 ± 5.65 kJ mol^{-1}) are close to the values for pseudo-hemicellulose reported in the literature, as 166.98 kJ mol^{-1} for rice straw, and 129.10 kJ mol^{-1} for sugarcane bagasse [8, 41]. For P-CL, an increase of E_a values comparable with that noted for hemicelluloses (P-HC1 and P-HC2) is observed in Table 2. The values obtained for P-CL are according to that estimate by Yang et al. [43] for microcrystalline cellulose, where the first step involves the formation of active cellulose (137.0 kJ mol^{-1}) and dehydrocellulose followed by active cellulose decomposition by two competitive formations of two volatiles (159.2 kJ mol^{-1} and 203.5 kJ mol^{-1}). The reported values are similar to those obtained for the cellulose of cocoa shell, where E_a is equal to 135.62 kJ mol^{-1} at the beginning of the reaction (formation of active cellulose) and 154.37 kJ mol^{-1} at the end of the reaction (active cellulose decomposition). For P-LG a significant increase in the E_a value occurred with the increase of conversion, resulting in a high value of E_a (201.42 ± 32.77 kJ mol^{-1}) when compared with the other pseudo-components. The increase was from 145.47 to 270.69 kJ mol^{-1}, which can be associated with the presence of several reactions that occur in parallel together with the high thermal stability of C–C bonds, thus needing more energy to break the chemical bonds. These high E_a values for pyrolysis of pseudo-lignin are reported for several biomasses (refer to Table 3), such as sugarcane bagasse (170.70 kJ mol^{-1}, average value)

Table 2 Apparent activation energy (E_a) values and thermodynamic parameters (ΔH, ΔG, and ΔS) calculated by the Vyazovkin method and activated complex theory for each independent pseudo-component at a different level of conversion

Component	Parameter	Conversion									Average[a,c]	ε^b(%)
		0.1	0.2	0.3	0.4	0.5	0.6	0.7	0.8	0.9		
P-ET	E_a (kJ mol^{-1})	100.57	99.86	100.72	101.96	103.39	105.01	106.88	109.20	112.60	104.56 (± 3.51)	0.78
	ΔH (kJ mol^{-1})	100.83	100.76	100.72	100.68	100.64	100.60	100.56	100.51	100.44	100.64 (± 0.10)	-
	ΔG (kJ mol^{-1})	133.29	133.84	134.25	134.61	134.94	135.27	135.63	136.06	136.64	134.95 (± 0.86)	-
	ΔS (J mol^{-1} K^{-1})	− 72.30	− 72.44	− 72.54	− 72.63	− 72.71	− 72.79	− 72.87	− 72.97	− 73.11	− 72.70 (± 0.21)	-
P-HC1	E_a (kJ mol^{-1})	133.71	139.81	144.37	148.34	152.12	155.96	160.12	165.06	172.05	152.41 (± 9.88)	0.42
	ΔH (kJ mol^{-1})	148.39	148.30	148.23	148.18	148.12	148.07	148.02	147.95	147.86	148.12 (± 0.14)	-
	ΔG (kJ mol^{-1})	143.50	143.39	143.31	143.25	143.19	143.13	143.06	142.99	142.89	143.19 (± 0.16)	-
	ΔS (J mol^{-1} K^{-1})	10.12	9.94	9.80	9.69	9.59	9.49	9.38	9.26	9.09	9.60 (± 0.27)	-
P-HC2	E_a (kJ mol^{-1})	128.63	132.26	134.92	137.24	139.40	141.58	143.94	146.70	150.59	139.48 (± 5.65)	0.31
	ΔH (kJ mol^{-1})	135.11	35.05	135.00	134.97	134.93	134.90	134.86	134.82	134.76	134.93 (± 0.09)	-
	ΔG (kJ mol^{-1})	155.72	156.00	156.20	156.38	156.54	156.70	156.88	157.08	157.37	156.54 (± 0.42)	-
	ΔS (J mol^{-1} K^{-1})	− 39.19	− 39.30	− 39.38	− 39.45	− 39.51	− 39.58	− 39.64	− 39.72	− 39.83	− 39.51 (± 0.16)	-
P-CL	E_a (kJ mol^{-1})	135.62	138.76	141.03	143.00	144.84	146.70	148.70	151.03	154.37	144.90 (± 4.80)	0.32
	ΔH (kJ mol^{-1})	140.14	140.08	140.05	140.01	139.98	139.95	139.92	139.88	139.83	139.98 (± 0.08)	-
	ΔG (kJ mol^{-1})	172.97	173.33	173.59	173.82	174.03	174.24	174.46	174.73	175.09	174.03 (± 0.55)	-
	ΔS (J mol^{-1} K^{-1})	− 57.33	− 57.42	− 57.49	− 57.54	− 57.60	− 57.65	− 57.70	− 57.77	− 57.85	− 57.59 (± 0.13)	-
P-LG	E_a (kJ mol^{-1})	145.47	159.45	172.48	184.93	197.44	210.68	225.56	243.85	270.69	201.42 (± 32.77)	0.25
	ΔH (kJ mol^{-1})	197.01	196.71	196.48	196.28	196.10	195.92	195.72	195.49	195.17	196.10 (± 0.47)	-
	ΔG (kJ mol^{-1})	179.96	178.78	177.92	177.19	176.52	175.85	175.13	174.30	173.17	176.54 (± 1.75)	-
	ΔS (J mol^{-1} K^{-1})	32.21	31.65	31.26	30.94	30.64	30.36	30.07	29.74	29.31	30.69 (± 0.75)	-

[a] Average calculated using the kinetic and thermodynamic parameters for all conversion data (variation of 0.001)

[b] Relative error calculated from the relationship between the right and left side of Eq. 4 by $\varepsilon = 100*(|\text{left side} - \text{right side}|)/\text{right side}$

[c] ±Average absolute deviation

[8], pine-fruit shell (309.38 kJ mol^{-1}, average value) [3], and açaí seed waste (346.24 kJ mol^{-1}, average value) [6].

3.3.2 Evaluation of the reaction model

The master plot method is used to distinguish the most probable devolatilization reaction pathway of each pseudo-component related to cocoa shell pyrolysis, as shown in Fig. 3b. The overlap between experimental and theoretical curves of the master plot revealed the most appropriate reaction model for each pseudo-component at the cocoa shell pyrolysis (P-ET, P-HC1, P-HC2, and P-LG). From the master plot results, different reaction mechanisms were identified for the pyrolysis of cocoa shell, which confirms its inherent multistep kinetics characteristic. The reaction model was described by the *n*-order models as the major component, except for the P-CL (R2: contracting cylinder). Low values of relative error were observed for P-ET ($\varepsilon = 0.12\%$), P-HC1 ($\varepsilon = 0.09\%$), P-HC2 ($\varepsilon = 0.19\%$), P-CL ($\varepsilon = 0.24\%$), and P-LG ($\varepsilon = 0.56\%$), suggesting a good application of these models to describe the pyrolysis of the pseudo-components present in the cocoa shell.

The devolatilization reaction mechanism of primary and secondary hemicelluloses (PS-HC1 and PS-HC2, respectively) can be inferred to be a second-order reaction model (F2) and first-order reaction model (F1), respectively. It was verified that the devolatilization of PS-ET followed the first-order reaction model (F1). For the *n*-order reaction mechanism, the devolatilization corresponds to the concentration of reactant raised to a specific power *n* [16]. Particularly, an eighth-order reaction model (F8) was found for P-LG, which implies a low collision probability. One could speculate that given the inherent characteristic of lignin structure, which involves a complex and rigid cross-linked phenolic structure, lignin pyrolysis is often associated with the combined effects of several mechanisms such as nucleation, diffusion, and power-law mechanism [20, 44]. Thus, it is reported that the high reaction order for lignin pyrolysis is a result of this combined effect. Chen et al. [45] observed that reaction orders between 6 and 8 could represent the pseudo-lignin of bamboo waste. For P-CL, the contracting model suggests that the quick nucleation controls the decomposition from the external surface toward the center of the sample. The occurrence the several parallel reactions

Table 3 Comparison of apparent activation energy and thermodynamics parameters for cocoa shell pyrolysis with literature values for lignocellulosic biomass pyrolysis

Reference	Feedstock	Kinetic method	E_a (kJ mol^{-1})	ΔH (kJ mol^{-1})	ΔG (kJ mol^{-1})	ΔS (J mol^{-1} K^{-1})
This study	Cocoa shell	Multistep kinetics (Vyazovkin)	104.56 for P-ET, 152.41 for P-HC1, 139.48 for P-HC2, 144.90 for P-CL, 201.42 for P-LG	100.64 for P-ET, 148.12 for P-HC1, 134.93 for P-HC2, 139.98 for P-CL, 196.10 for P-LG	134.95 for P-ET, 143.19 for P-HC1, 156.54 for P-HC2, 174.03 for P-CL, 176.54 for P-LG	−72.70 for P-ET, 9.60 for P-HC1, −39.51 for P-HC2, −57.59 for P-CL, 30.69 for P-LG
Ref. [3]	Pine-fruit shell	Multistep kinetics (Vyazovkin)	179.00 for P-HC, 201.02 for P-CL, 309.38 for P-LG	174.31 for P-HC, 196.05 for P-CL, 303.21 for P-LG	158.09 for P-HC, 173.13 for P-CL, 180.09 for P-LG	28.77 for P-HC, 38.31 for P-CL, 166.13 for P-LG
Ref. [6]	Açaí seed	Multistep kinetics (Vyazovkin)	103.95 for P-HC, 135.01 for P-CL, 346.24 for P-LG	99.13 for P-HC, 129.38 for P-CL, 338.54 for P-LG	164.27 for P-HC, 180.27 for P-CL, 199.75 for P-LG	−115.00 for P-HC, −77.55 for P-CL, 162.02 for P-LG
Ref. [8]	Sugarcane bagasse	Multistep kinetics (Starink-1.92)	130.80 for P-ET, 129.10 for P-HC, 136.40 for P-CL, 170.70 for P-LG	-	-	-
Ref. [8]	Cashew nut shells	Multistep kinetics (Starink-1.92)	83.20 for P-ET, 109.80 for P-HC, 114.40 for P-CL, 155.40 for P-LG	-	-	-
Ref. [41]	Rice straw	Multistep kinetics (FWO)	166.98 for P-HC, 178.47 for P-CL	162.24 for P-HC, 173.30 for P-CL	164.60 for P-HC, 180.14 for P-CL	−4.13 for P-HC, −11.01 for P-CL
Ref. [41]	Rice bran	Multistep kinetics (FWO)	115.12 for P-HC, 164.78 for P-CL	111.03 for P-HC, 159.96 for P-CL	141.62 for P-HC, 167.18 for P-CL	−62.15 for P-HC, −12.46 for P-CL
Ref. [42]	Castor residue	Single-step kinetics (FWO)	167.10	162.15	152.05	-

following different mechanisms is widely reported in lignocellulosic biomass pyrolysis [46, 47].

3.3.3 Estimation of pre-exponential factors

The knowledge of the pre-exponential factor is essential to extract information about the chemical reaction of pyrolysis and critical to optimize the biomass pyrolysis [48, 49]. As previously discussed, the overall behavior of cocoa shell pyrolysis can be interpreted as five parallel devolatilization reactions. For each pseudo-component, a high linear relation between the apparent activation energy (obtained using Vyazovkin method) and pre-exponential factor (in its natural logarithmic form, ln$A$) was confirmed by a high correlation coefficient ($R^2 > 0.9546$ for all pseudo-components as shown in Fig. 3a). The occurrence of the compensation effect in cocoa shell pyrolysis corroborates that this method is reasonably able to deliver representative pre-exponential factors.

The values of ln(A) for P-ET, P-HC1, P-HC2, P-CL, and P-LG, are 26.27, 36.25, 30.41, 28.31, and 39.00, respectively. The pre-exponential factors for the five pseudo-components are in the range of 2.56×10^{11} to 8.66×10^{16} min^{-1} (2.55×10^{11} min^{-1}, 5.55×10^{15} min^{-1}, 1.60×10^{13} min^{-1}, 1.97×10^{12} min^{-1}, and 8.65×10^{16} min^{-1} for P-ET, P-HC1, P-HC2, P-CL, and P-LG, respectively), which are comparable with the range found for sub-bituminous coal, açaí seed waste, and reed canary [6, 50, 51]. The fluctuations are related to the magnitude of the pre-exponential factors that suggest a complex devolatilization reaction and confirm the hypothesis of several parallel devolatilization reactions [42, 52]. The values of A calculated from Eq. 6, which is based on the Kissinger's method, are shown in Table 4.

The values of A obtained from ASTM E698-18 (Eq. 6) were near in power to values estimated by the compensation method. The values of A for P-ET and P-HC2 were similar in both methods with a difference of 7.69% and 6.36%, respectively, when compared with the values of A estimated from compensation effect. This similar data can be associated with the reaction model identified for this pseudo-component (P-ET and P-HC2), which was F1 that is the same used on the assumption of Kissinger's method. On the other hand, the values of A for P-HC1, P-CL, and P-LG were different than those obtained from the compensation effect, with a difference of 55.12%, 104.72%, and 73.80%, respectively. The dissimilar result can be associated with considerations applied in Eq. 6 (ASTM E698-18), such as assuming the reaction model as a first-order reaction, which is not true since each pseudo-component presents its respective model. This different value may reflect in a deviation between the experimental and simulated data.

From the five kinetic triplets obtained, an overall kinetic differential equation was considered as the sum of the contributions of all pseudo-components to reconstruct the kinetically complex of cocoa shell pyrolysis.

Fig. 3 **a** Compensation effect plots (ln(A) versus E_a) and **b** experimental and theoretical curves ($g(\alpha)/g(0.5)$ versus α) using the master plot method (for each independent pseudo-component)
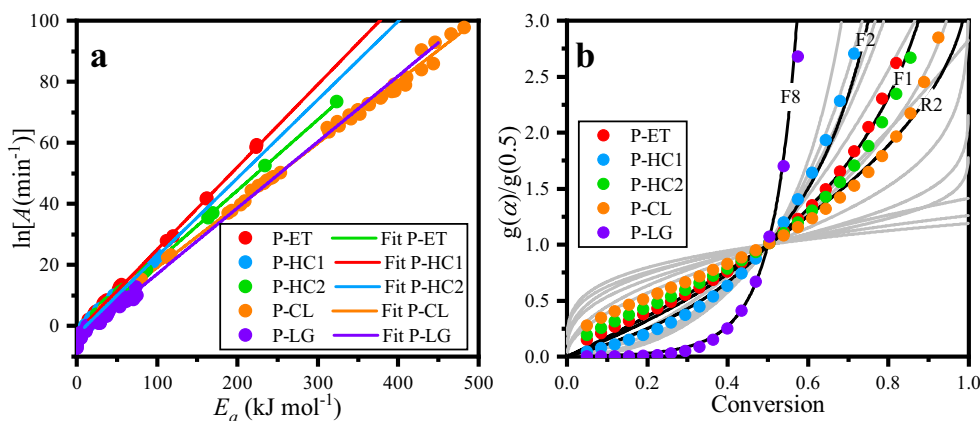
3.3.4 Verification of the overall kinetic expression

The thermal decomposition curves (dα/dt *versus T*) were reconstructed and compared with the experimental data to verify the accuracy of overall kinetic expression. For this, it was assumed that the pyrolysis of the cocoa shell is represented by the contribution of the five independent parallel reactions. Thus, the overall pyrolysis can be described mathematically using the kinetic triplet previously estimated. Equation 19 uses the kinetic data with A values calculated from the compensation method, while Eq. 20 uses the kinetic data with A values calculated from Kissinger's method. This verification is essential to ensure that the overall kinetic expression obtained can be used in the design and simulation of cocoa shell pyrolysis and is aligned with recently published recommendations of the ICTAC Kinetics Committee for the kinetic analysis of overlapping multistep reactions [53].

$$\left(\frac{d\alpha}{dt}\right)_{Biomass} = \sum_{i=1}^{N} c_i \left(\frac{d\alpha}{dt}\right)_i = \begin{cases} c_{P-ET}\left(2.53x10^{11}\right)e^{-104560/RT}(1-\alpha) \\ c_{P-HC1}\left(5.54x10^{15}\right)e^{-152410/RT}(1-\alpha)^2 \\ c_{P-HC2}\left(1.61x10^{13}\right)e^{-139480/RT}(1-\alpha) \\ c_{P-CL}\left(1.97x10^{12}\right)e^{-144900/RT}\left[2(1-\alpha)^{1/2}\right] \\ c_{P-LG}\left(8.66x10^{16}\right)e^{-201420/RT}(1-\alpha)^8 \end{cases}$$

(19)

$$\left(\frac{d\alpha}{dt}\right)_{Biomass} = \sum_{i=1}^{N} c_i \left(\frac{d\alpha}{dt}\right)_i = \begin{cases} c_{P-ET}\left(2.74x10^{11}\right)e^{-104560/RT}(1-\alpha) \\ c_{P-HC1}\left(2.48x10^{15}\right)e^{-152410/RT}(1-\alpha)^2 \\ c_{P-HC2}\left(1.49x10^{13}\right)e^{-139480/RT}(1-\alpha) \\ c_{P-CL}\left(4.05x10^{12}\right)e^{-144900/RT}\left[2(1-\alpha)^{1/2}\right] \\ c_{P-LG}\left(2.26x10^{16}\right)e^{-201420/RT}(1-\alpha)^8 \end{cases}$$

(20)

The individual contribution fraction (c_i) for each pseudo-component during the pyrolysis of cocoa shell waste was 0.1250, 0.0992, 0.1697, 0.2103, and 0.3977 for P-ET, P-HC1, P-HC2, P-CL, and P-LG, respectively. Based on these data, the simulated curves were plotted by solving Eq. 19 and Eq. 20 with the numerical method of Runge-Kutta fourth-order. Figures 4 and 5 indicate that the use of the Kissinger's method by ASTM E698-18 to estimate the pre-exponential factor does not reproduce the experimental data completely, differently from that observed for compensation effect. The thermal behavior between 423 and 555 K and temperatures above 698 K were reproduced using the values of A calculated by Eq. 6 (ASTM E698-18); however, there is a large deviation between reconstructed and experimental curves. The determination coefficient for curves obtained from Eq. 20 ($R^2 = 0.5740–0.6938$) was lower than that obtained from Eq. 19 ($R^2 = 0.9446–0.9749$), which indicates a better reproduction of the experimental data by the kinetic parameters estimated using Eq. 19. The RSS is another important parameter to verify both proposed overall kinetic expressions

Table 4 Pre-exponential factor calculated using the ASTM E698-18 based on Kissinger's method

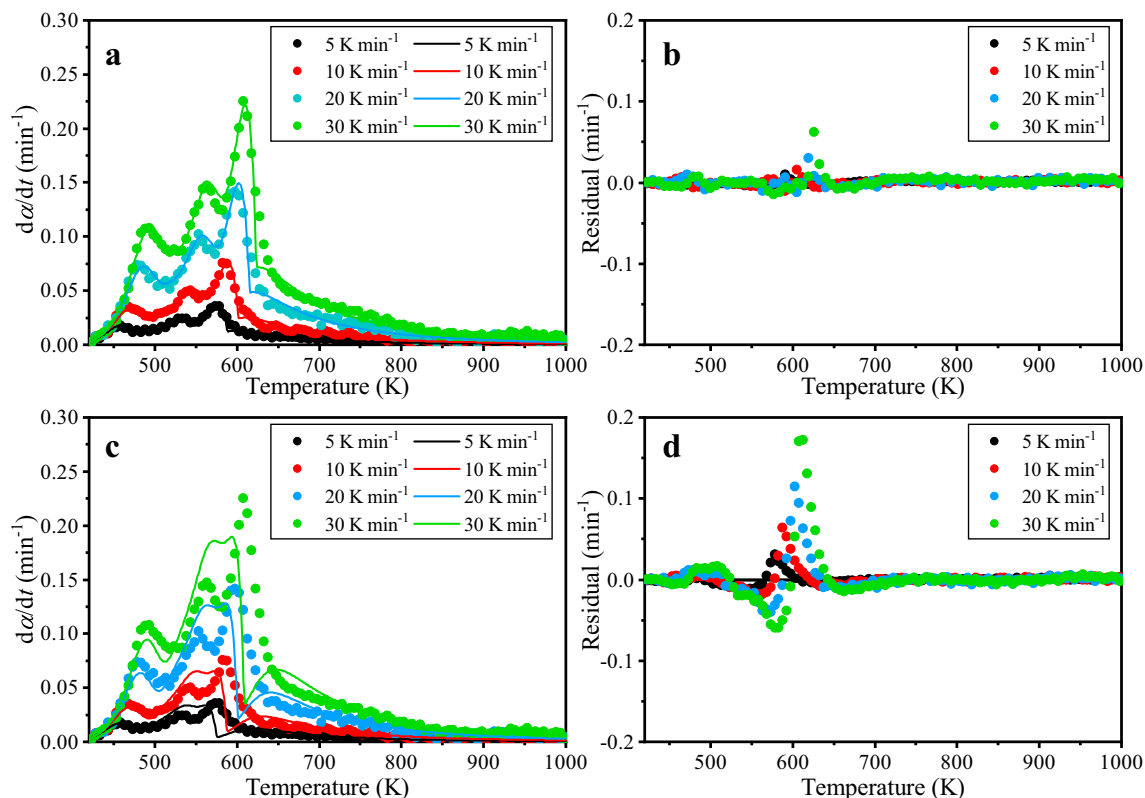| β (K min^{-1})	Pre-exponential factor (min^{-1})				
	P-ET	P-HC1	P-HC2	P-CL	P-LG
5	2.66×10^{11}	2.23×10^{15}	1.43×10^{13}	3.86×10^{1}	2.27×10^{16}
10	2.92×10^{11}	2.68×10^{15}	1.56×10^{13}	4.23×10^{12}	2.38×10^{16}
20	2.90×10^{11}	2.78×10^{15}	1.57×10^{13}	4.26×10^{12}	2.31×10^{16}
30	2.48×10^{11}	2.23×10^{15}	1.42×10^{13}	3.84×10^{12}	2.08×10^{16}
Average	2.74×10^{11}	2.48×10^{15}	1.49×10^{13}	4.05×10^{12}	2.26×10^{16}
ln(A) (ln(min^{-1}))					
Average	26.34	35.45	30.34	29.03	37.66

Fig. 4 (-) Reconstructed and (•) experimental curves (dα/dt *versus T*) at four heating rates and residual for **a–b** Eq. 19 and **c–d** Eq. 20

(one with *A* values calculated from the compensation method and another with *A* values calculated from Kissinger's method). The *RSS* data for Eq. 19 (*RSS* = 0.0024–0.0418) was lower than that of Eq. 20 (*RSS* = 0.0182–0.5760), i.e., the difference between simulated and experimental data is lower for Eq. 19 compared with Eq. 20. According to Fig. 5b, the pseudo-components described by the first-order model (P-ET and P-HC2) were properly described, while the pseudo-component (P-CL) that is not described by an *n*-reaction cannot be described. Considerations used to obtain Eq. 6 represent the main factor for the inability to reproduce the experimental behavior. The use of Kissinger's method reduced the *QOF* values due to the consideration of the first-order reaction to calculate all values of *A*, where a difference of 5.9549–6.2609 was observed between the *QOF* of both methods. According to ASTM E698-18 [9], the technique may not work with reactions that include simultaneous or consecutive reaction steps; thus, Eq. 20 should not be considered, and the Kissinger's method is not suitable for indicating the values of *A*. Figure 4c indicates that Kissinger's method should only be used when the reaction model is represented by first-order reactions. Figures 4a and 5a show a successful description of the overall process of devolatilization from Eq. 19 for ligno-cellulosic biomass with high complexity, such as cocoa shell waste. The curves provided by Eq. 19 describe the thermal behavior of cocoa shell waste pyrolysis properly. In Fig. 4, it is noted that the thermal behavior provided from Eq. 19 could describe most of the decomposition region, where a small region

(Fig. 4b–c) between 600 and 640 K presented a low adjustment, although the low difference between the residual mean (Fig. 5). At this temperature range, the curves calculated from Eq. 20 did not show a good fit, indicating the non-applicability of the Kissinger's method for estimating *A* values for reactions not represented by a first order.

These results indicate the validity of the kinetic triplet estimated from the Vyazovkin method, compensation effect, and master plot, where these data describe as closely as possible the real decomposition process of cocoa shell waste. Besides, the reconstruction of the experimental thermogravimetric curves using the kinetic triplet, with *A* values estimated from compensation parameters, is hardly found in the literature, which is essential for application in thermochemical systems and prediction of thermal decomposition curves.

3.4 Qualitative evaluation of volatile pyrolysis products

The 3D-FTIR spectrum of the evolved volatile products from the pyrolysis of the cocoa shell is shown in Fig. 6a. Based on this data, the FTIR spectrums (Fig. 6b) were selected at temperatures of 362 K, 483 K, 551 K, 600 K, 690 K, and 773 K for the identification of the products. Finally, Fig. 6c shows the evolution of the main volatile products as a function of temperature.
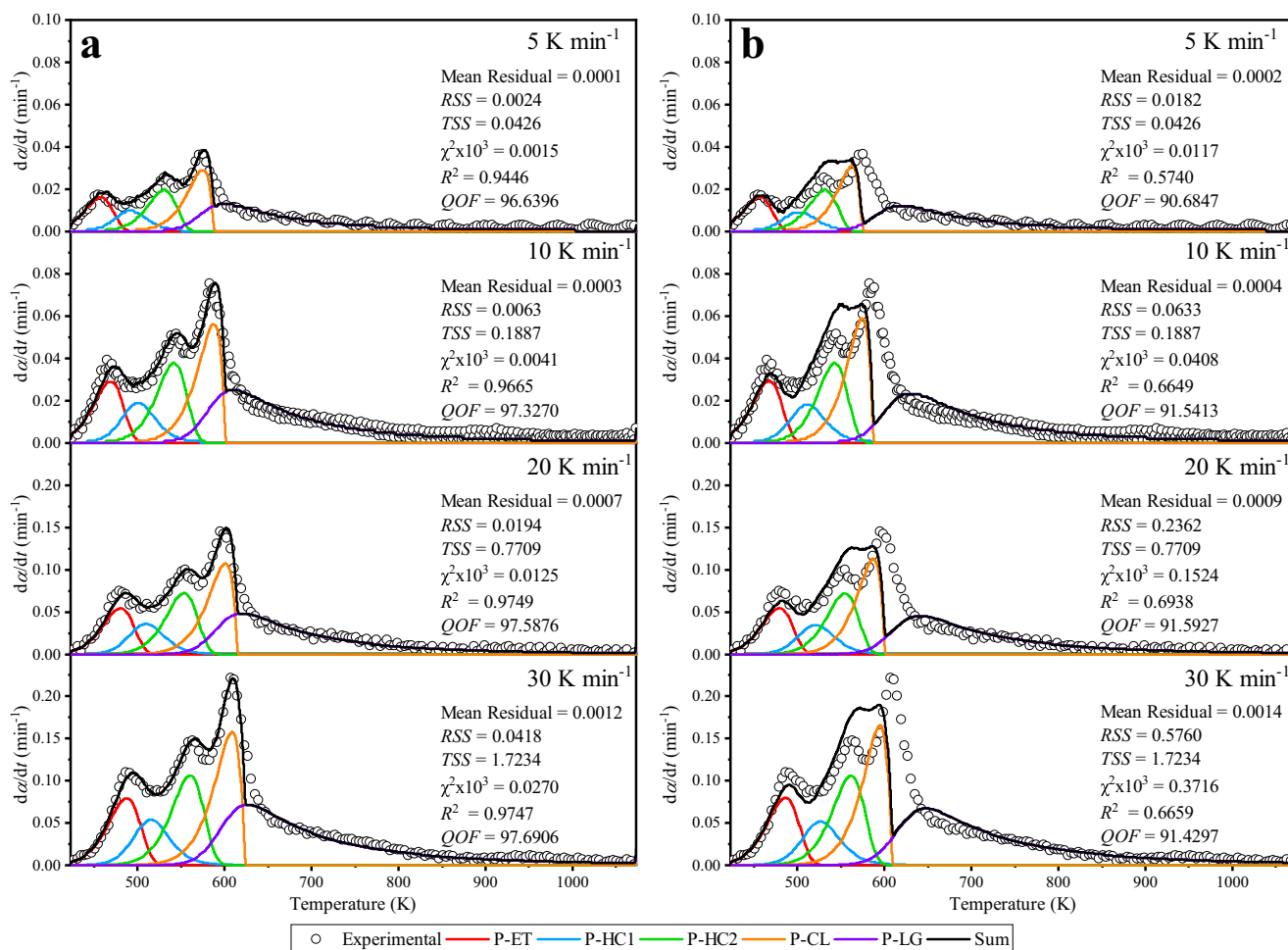
Fig. 5 Overlap of predicted curves of P-ET, P-HC1, P-HC2, P-CL, and P-LG obtained from **a** Eq. 19 and **b** Eq. 20 for heating rates of 5, 10, 20, and 30 K min^{-1} with their respective statistical analysis

The FTIR spectrums indicated the generation of the following volatile species: H_2O (water), $H_3C–OH$ (alcohols), $H_3C–O–CH_3$ (ethers), $H_3C–CH_3$ (alkanes), $C \equiv O$ (carbon monoxide), $O=C=O$ (carbon dioxide), $H_3C–CH=O$ (aldehyde, ketones or esters), and CH_4 (methane). As observed in Fig. 6c, the volatile products H_2O, alcohol, ether, CO_2, CO, and aldehyde/ketones/esters evolved at a wide temperature range with an evolution profile that agrees with the pyrolysis behavior (DTG). The peaks between 3800 and 3500 cm^{-1} are associated with the symmetric and asymmetric stretching vibrations of H_2O molecules, which decreases its intensity with increasing temperature [17]. The presence of H_2O molecules was also identified in the band between 1550 and 1400 cm^{-1}. The release of CO_2 is observed in the strong band between 2400 and 2240 cm^{-1}, with the main contribution related to the cracking of functional groups of hemicellulose at temperatures below 700 K [54]. The peak at 2200–2000 cm^{-1} is a characteristic of CO and is derived from the cracking of lignocellulosic components via decarboxylation, which disappears in temperatures above 700 K [3]. The bands at 1000–1300 cm^{-1} are attributed to oxygen functional groups ($H_3C–OH$ and $H_3C–$

$O–CH_3$), which decompose mainly into CO_2 by reformation or cracking at temperatures above 600 K. The bands in the range of 3100–2700 cm^{-1} can be associated with different organic compounds, including hydrocarbons (alkanes: $H_3C–CH_3$) and different oxygenated compounds (alcohols: $H_3C–OH$ and ethers: $H_3C–O–CH_3$), which are formed during the devolatilization of the cocoa shell mainly between 400 and 600 K. In this band region, the presence of alkanes is resulting from symmetrical and asymmetrical CH stretching bands of the aliphatic CH_3 and CH_2 groups. The peak at the range of 1600–1800 cm^{-1} is characterized by C=O stretching vibrations of the carboxylic acid or carbonyl compounds, corresponding to functional groups of aldehydes, ketones, and esters, which occur principally between 400 and 600 K. The bands between 3140 and 2700 cm^{-1} are characteristic of CH_4, which is released from the lignin by pyrolytic cracking of aromatic compounds at temperatures above 600 K [17]. Figure 6c showed that the concentrations of evolved volatile products follow the order: CO_2 > aldehyde/ketones/esters > ether > H_2O > alcohol > CO > CH_4, when it is considered a linear relationship between absorbance intensity and
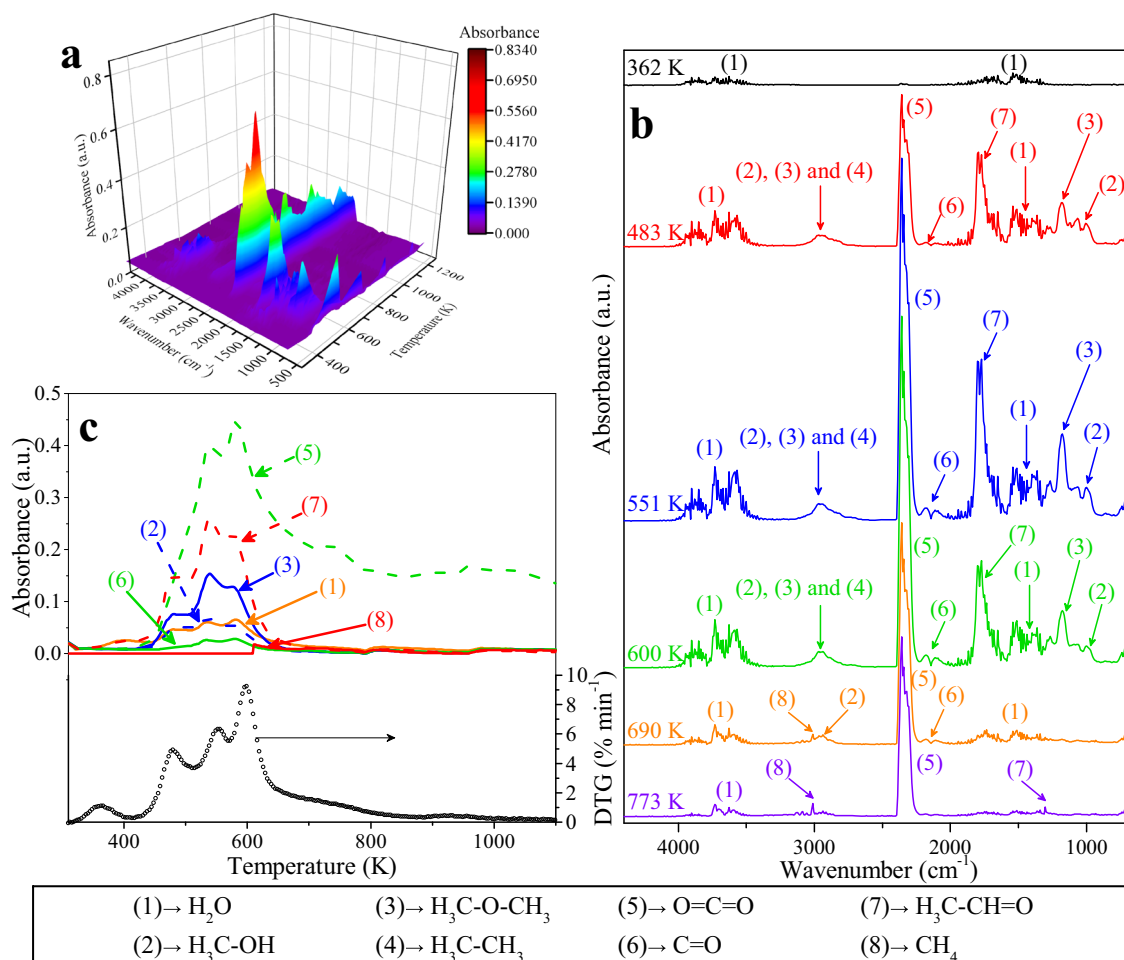
Fig. 6 **a** 3D-FTIR spectrum of the evolved volatile products from the pyrolysis of the cocoa shell; **b** FTIR spectrums at several selected temperatures according to DTG analysis; and **c** evolution of volatile products as a function of temperature compared with DTG analysis

concentration. These volatile species are typical in the pyrolysis of lignocellulosic biomass [3, 17, 55].

3.5 Thermodynamic implications

The thermodynamic parameters of the thermochemical conversion of biomass give valuable information regarding its feasibility and energy requirements. For practical purposes, the thermodynamic parameters can be used as valuable inputs in prediction models of resulting gaseous emissions from biomass thermochemical conversion [56]. Thermodynamic parameters evaluation can also support the definition of operating conditions. Tahir et al. [57] reported that an energetically favorable pyrolytic conversion of canola residue biomass to biofuel is expected for low temperatures (< 450 °C), taking into account the kinetic and thermodynamic findings. The values of E_a obtained using Vyazovkin method were employed to derive the thermodynamics parameters of the lignocellulosic pseudo-components. Table 2 shows the thermodynamic parameters as a function of the degree of conversion for each pseudo-component.

The ΔH value is an estimate of the energy consumed by pyrolysis to convert the cocoa shell into bioenergy products. According to Daugaard and Brown [58], the reactor sizing and design of an efficient system depend on heat transfer issues and energy required by the biomass during pyrolysis. Table 2 shows positive ΔH values (100.64 ± 0.10 kJ mol^{-1} for P-ET, 148.12 ± 0.14 kJ mol^{-1} for P-HC1, 134.93 ± 0.09 kJ mol^{-1} for P-HC2, 139.98 ± 0.08 kJ mol^{-1} for P-CL, and 196.10 ± 0.47 kJ mol^{-1} for P-LG) that indicates an endothermic nature for all pseudo-components. The comparison between the thermodynamic parameters for the five pseudo-components in cocoa shell pyrolysis and literature values for the pyrolysis of different kinds of biomasses is previously shown in Table 3. As noted in Table 3, the ΔH values for cocoa shell waste are in good agreement with other lignocellulosic biomass such as pine-fruit shell, rice straw, rice bran, and castor residue [3, 41, 42], which implies that the pyrolytic conversion of the cocoa shell can be competitive with these lignocellulosic feedstocks. In addition, the difference between ΔH and E_a is referred to as "potential energy barrier," where the values found were below 5.50 kJ mol^{-1} for all pseudo-components.

This value indicates a feasible reaction to produce bioenergy from the cocoa shell pyrolysis since small additional energy is required to achieve product generation [15].

The ΔG value represents the available bioenergy recovered from the pyrolysis of the cocoa shell. The positive value of ΔG for all pseudo-components varied from 134.95 to 176.54 kJ mol^{-1}, with results comparable with related literature (see Table 3) [3, 41, 42]. The signals of thermodynamics functions validated the devolatilization of the cocoa shell as a non-spontaneous process; thus, the process requires a significant amount of energy to convert the cocoa shell into bioenergy products.

Negative values of ΔS demonstrate that pseudo-components P-ET ($-$ 72.70 $\pm$ 0.21 J mol^{-1} K^{-1}), P-HC2 ($-$ 39.51 $\pm$ 0.16 J mol^{-1} K^{-1}), and P-CL ($-$ 57.59 $\pm$ 0.13 J mol^{-1} K^{-1}) are close to their thermodynamic equilibrium, i.e., present higher thermodynamic stability. Therefore, the level of disorder of products by the volatile release was lower than that of the initial reactants, requiring more time to achieve the activated complex [16]. In contrast, the positive ΔS value indicates a high reactivity in the pseudo-components P-HC1 (9.60 $\pm$ 0.27 J mol^{-1} K^{-1}) and P-LG (30.69 $\pm$ 0.75 J mol^{-1} K^{-1}), which consume less time to form the activated complex from volatiles release and molecular rearrangement. ΔS values for pseudo-components are fluctuating between positive and negative signals during the pyrolysis for the cocoa shell, which can indicate a complex reaction to produce bioenergy. This is a typical behavior for the pyrolysis of lignocellulosic biomass [5, 42]. Thermodynamic properties suggested that the cocoa shell waste is an interesting candidate for bioenergy conversion through pyrolysis.

4 Conclusions

In this study, the cocoa shell was presented as a new renewable feedstock for pyrolysis due to its abundance and physicochemical characteristics. It was demonstrated that the cocoa shell is a renewable source for bioenergy production potentially exploitable due to the values of HHV (17.21 MJ kg^{-1}), high bulk density (581.25 kg m^{-3}), and low contents of ash (6.79 wt%) and sulfur (0.01 wt%), which can compete with conventional bioenergy feedstocks. The nonisothermal thermogravimetry, coupled to the evolved gas analysis, provided insights on the cocoa shell pyrolysis, where it demonstrated a multistep conversion process. The reliable description of the entire conversion process of the cocoa shell in the form of kinetic triplet and thermodynamic parameters is of great importance to design an effective reactor; for this, isoconversional kinetic evaluation combined with a symmetrical deconvolution analysis was successfully adopted to describe the multistep kinetics with low discrepancies.

Regarding the estimation of the pre-exponential factor, the compensation effect method (ranging from 2.56 $\times$ 10^{11} min^{-1} to 8.66 $\times$ 10^{16} min^{-1}) and Kissinger's expression (ranging from 2.74 $\times$ 10^{11} min^{-1} to 2.26 $\times$ 10^{16} min^{-1}) provided different values of A, and experimental curves critically compared these data. It was noted that Kissinger's method, when used for the estimation of A values, does not reproduce the experimental behavior, which can be associated with several limitations, as the assumption of a first-order reaction. This finding is in a reasonable agreement with ICTAC Kinetics Committee recommendations and ASTM E698-18. On the other hand, the compensation effect method can deal with multistep kinetics, which implies multiple kinetic triplets, as indicated by the excellent agreement between experimental curves and reconstructed curves using the isoconversional kinetic evaluation combined with the symmetrical deconvolution analysis ($R^2 > 0.9446$).

References

1. FAOSTAT (2020) Cocoa Beans (Crops Production). Food and agriculture organization of the United Nations (Statistics Division). Available: <http://www.fao.org/faostat/en/#data>. (Accessed 10 February 2020)

2. Vásquez ZS, de Carvalho Neto DP, Pereira GVM, Vandenberghe LPS, de Oliveira PZ, Tiburcio PB, Rogez HLG, Góes Neto A, Soccol CR (2019) Biotechnological approaches for cocoa waste management: a review. Waste Manag 90:72–83. https://doi.org/10.1016/j.wasman.2019.04.030

3. Alves JLF, Da Silva JCG, da Silva Filho VF et al (2019) Determination of the bioenergy potential of Brazilian pine-fruit shell via pyrolysis kinetics, thermodynamic study, and evolved gas analysis. Bioenergy Res 12:168–183. https://doi.org/10.1007/s12155-019-9964-1

4. Chen J, Wang Y, Lang X, Ren X', Fan S (2017) Evaluation of agricultural residues pyrolysis under non-isothermal conditions: thermal behaviors, kinetics, and thermodynamics. Bioresour Technol 241:340–348. https://doi.org/10.1016/j.biortech.2017.05.036

5. Fernandez A, Ortiz LR, Asensio D, Rodriguez R, Mazza G (2020) Kinetic analysis and thermodynamics properties of air/steam gasification of agricultural waste. J Environ Chem Eng 8:103829. https://doi.org/10.1016/j.jece.2020.103829

6. Alves JLF, Da Silva JCG, Di Domenico M et al (2020) Exploring Açaí seed (Euterpe oleracea) pyrolysis using multi-component kinetics and thermodynamics assessment towards its bioenergy potential. BioEnergy Res. https://doi.org/10.1007/s12155-020-10175-y

7. Vyazovkin S, Wight CA (1999) Model-free and model-fitting approaches to kinetic analysis of isothermal and nonisothermal data.

Thermochim Acta 340–341:53–68. https://doi.org/10.1016/S0040-6031(99)00253-1

8. da Silva JCG, de Albuquerque JG, Galdino WV d A et al (2020) Single-step and multi-step thermokinetic study – deconvolution method as a simple pathway for describe properly the biomass pyrolysis for energy conversion. Energy Convers Manag 209:112653. https://doi.org/10.1016/j.enconman.2020.112653

9. ASTM (2018) E698-18: Kinetic parameters for thermally unstable materials using differential scanning calorimetry and the Flynn/Wall/Ozawa method. In: Annual Book of ASTM Standards. ASTM International, West Conshohocken, pp 1–9. https://doi.org/10.1520/E0698-18

10. Vyazovkin S, Burnham AK, Criado JM, Pérez-Maqueda LA, Popescu C, Sbirrazzuoli N (2011) ICTAC Kinetics Committee recommendations for performing kinetic computations on thermal analysis data. Thermochim Acta 520:1–19. https://doi.org/10.1016/j.tca.2011.03.034

11. da Silva JCG, Alves JLF, Galdino WV d A et al (2018) Pyrolysis kinetic evaluation by single-step for waste wood from reforestation. Waste Manag 72:265–273. https://doi.org/10.1016/j.wasman.2017.11.034

12. Papadikis K, Gu S, Bridgwater AV, Gerhauser H (2009) Application of CFD to model fast pyrolysis of biomass. Fuel Process Technol 90:504–512. https://doi.org/10.1016/j.fuproc.2009.01.010

13. Ranganathan P, Gu S (2015) Computational fluid dynamics modelling of biomass fast pyrolysis in fluidised bed reactors, focusing different kinetic schemes. Bioresour Technol 213:333–341. https://doi.org/10.1016/j.biortech.2016.02.042

14. Boateng AA, Mtui PL (2012) CFD modeling of space-time evolution of fast pyrolysis products in a bench-scale fluidized-bed reactor. Appl Therm Eng 33–34:190–198. https://doi.org/10.1016/j.applthermaleng.2011.09.034

15. Mumbach GD, Alves JLF, Da Silva JCG et al (2019) Thermal investigation of plastic solid waste pyrolysis via the deconvolution technique using the asymmetric double sigmoidal function: determination of the kinetic triplet, thermodynamic parameters, thermal lifetime and pyrolytic oil composition for clean. Energy Convers Manag 200:112031. https://doi.org/10.1016/j.enconman.2019.112031

16. Alves JLF, Da Silva JCG, da Silva Filho VF et al (2019) Bioenergy potential of red macroalgae Gelidium floridanum by pyrolysis: evaluation of kinetic triplet and thermodynamics parameters. Bioresour Technol 291:121892. https://doi.org/10.1016/j.biortech.2019.121892

17. Lopez-Velazquez MA, Santes V, Balmaseda J, Torres-Garcia E (2013) Pyrolysis of orange waste: a thermo-kinetic study. J Anal Appl Pyrolysis 99:170–177. https://doi.org/10.1016/j.jaap.2012.09.016

18. Janković B, Manić N, Dodevski V, Popović J, Rusmirović JD, Tošić M (2019) Characterization analysis of Poplar fluff pyrolysis products. Multi-component kinetic study. Fuel 238:111–128. https://doi.org/10.1016/j.fuel.2018.10.064

19. Janković B, Manić N, Stojiljković D, Jovanović V (2018) TSA-MS characterization and kinetic study of the pyrolysis process of various types of biomass based on the Gaussian multi-peak fitting and peak-to-peak approaches. Fuel 234:447–463. https://doi.org/10.1016/j.fuel.2018.07.051

20. Wang X, Hu M, Hu W, Chen Z, Liu S, Hu Z, Xiao B (2016) Thermogravimetric kinetic study of agricultural residue biomass pyrolysis based on combined kinetics. Bioresour Technol 219:510–520. https://doi.org/10.1016/j.biortech.2016.07.136

21. Van de Velden M, Baeyens J, Brems A et al (2010) Fundamentals, kinetics and endothermicity of the biomass pyrolysis reaction. Renew Energy 35:232–242. https://doi.org/10.1016/j.renene.2009.04.019

22. ASTM (2014) E1131-08: Standard test method for compositional analysis by thermogravimetry. In: Annual Book of ASTM Standards. ASTM International, West Conshohocken, pp 1–6. https://doi.org/10.1520/E1131-08R14

23. ASTM (2008) D5373-08: Standard test methods for instrumental determination of carbon, hydrogen, and nitrogen in laboratory samples of coal. In: Annual Book of ASTM Standards. ASTM International, West Conshohocken, pp 1–9. https://doi.org/10.1520/D5373-08

24. ASTM (2017) D4239-17: Standard test method for sulfur in the analysis sample of coal and coke using high-temperature tube furnace combustion. In: Annual Book of ASTM Standards. West Conshohocken, pp 1–7. https://doi.org/10.1520/D4239-17

25. Van Soest PJ, Robertson JB, Lewis BA (1991) Methods for dietary fiber, neutral detergent fiber, and nonstarch polysaccharides in relation to animal nutrition. J Dairy Sci 74:3583–3597. https://doi.org/10.3168/jds.S0022-0302(91)78551-2

26. Alves JLF, da Silva JCG, Mumbach GD, Domenico MD, de Sena RF, Machado RAF, Marangoni C (2020) Demonstrating the suitability of tamarind residues to bioenergy exploitation via combustion through physicochemical properties, performance indexes, and emission characteristics. BioEnergy Res. https://doi.org/10.1007/s12155-020-10158-z

27. ASTM (2013) D5865-13: Standard test method for gross calorific value of coal and coke. In: Annual Book of ASTM Standards. ASTM International, West Conshohocken, pp 1–19. https://doi.org/10.1520/D5865-13

28. ASTM (2019) E873-82: Standard test method for bulk density of densified particulate biomass fuels. In: Annual Book of ASTM Standards. ASTM International, West Conshohocken, pp 1–2. https://doi.org/10.1520/E0873-82R19

29. Kim YS, Kim YS, Kim SH (2010) Investigation of thermodynamic parameters in the thermal decomposition of plastic waste-waste lube oil compounds. Environ Sci Technol 44:5313–5317. https://doi.org/10.1021/es101163e

30. Frau C, Ferrara F, Orsini A, Pettinau A (2015) Characterization of several kinds of coal and biomass for pyrolysis and gasification. Fuel 152:138–145. https://doi.org/10.1016/j.fuel.2014.09.054

31. García R, Pizarro C, Lavín AG, Bueno JL (2012) Characterization of Spanish biomass wastes for energy use. Bioresour Technol 103:249–258. https://doi.org/10.1016/j.biortech.2011.10.004

32. Kalkreuth W, Holz M, Kern M, Machado G, Mexias A, Silva MB, Willett J, Finkelman R, Burger H (2006) Petrology and chemistry of Permian coals from the Paraná Basin: 1. Santa Terezinha, Leão-Butiá and Candiota Coalfields, Rio Grande do Sul, Brazil. Int J Coal Geol 68:79–116. https://doi.org/10.1016/j.coal.2005.10.006

33. Mythili R, Venkatachalam P, Subramanian P, Uma D (2013) Characterization of bioresidues for biooil production through pyrolysis. Bioresour Technol 138:71–78. https://doi.org/10.1016/j.biortech.2013.03.161

34. Titiloye JO, Abu Bakar MS, Odetoye TE (2013) Thermochemical characterisation of agricultural wastes from West Africa. Ind Crops Prod 47:199–203. https://doi.org/10.1016/j.indcrop.2013.03.011

35. Merdun H, Sezgin İV (2018) Products distribution of catalytic co-pyrolysis of greenhouse vegetable wastes and coal. Energy 162:953–963. https://doi.org/10.1016/j.energy.2018.08.004

36. Ceylan S, Topçu Y (2014) Pyrolysis kinetics of hazelnut husk using thermogravimetric analysis. Bioresour Technol 156:182–188. https://doi.org/10.1016/j.biortech.2014.01.040

37. Biagini E, Fantei A, Tognotti L (2008) Effect of the heating rate on the devolatilization of biomass residues. Thermochim Acta 472:55–63. https://doi.org/10.1016/j.tca.2008.03.015

38. Yuan T, Tahmasebi A, Yu J (2015) Comparative study on pyrolysis of lignocellulosic and algal biomass using a thermogravimetric and a fixed-bed reactor. Bioresour Technol 175:333–341. https://doi.org/10.1016/j.biortech.2014.10.108

39. Chen Z, Hu M, Zhu X, Guo D, Liu S, Hu Z, Xiao B, Wang J, Laghari M (2015) Characteristics and kinetic study on pyrolysis of five lignocellulosic biomass via thermogravimetric analysis. Bioresour Technol 192:441–450. https://doi.org/10.1016/j.biortech.2015.05.062

40. Várhegyi G (2007) Aims and methods in non-isothermal reaction kinetics. J Anal Appl Pyrolysis 79:278–288. https://doi.org/10.1016/j.jaap.2007.01.007

41. Xu Y, Chen B (2013) Investigation of thermodynamic parameters in the pyrolysis conversion of biomass and manure to biochars using thermogravimetric analysis. Bioresour Technol 146:485–493. https://doi.org/10.1016/j.biortech.2013.07.086

42. Kaur R, Gera P, Jha MK, Bhaskar T (2018) Pyrolysis kinetics and thermodynamic parameters of castor (Ricinus communis) residue using thermogravimetric analysis. Bioresour Technol 250:422–428. https://doi.org/10.1016/j.biortech.2017.11.077

43. Yang X, Zhao Y, Li R, Wu Y, Yang M (2018) A modified kinetic analysis method of cellulose pyrolysis based on TG–FTIR technique. Thermochim Acta 665:20–27. https://doi.org/10.1016/j.tca.2018.05.008

44. Yeo JY, Chin BLF, Tan JK, Loh YS (2017) Comparative studies on the pyrolysis of cellulose, hemicellulose, and lignin based on combined kinetics. J Energy Inst. 92:27–37. https://doi.org/10.1016/j.joei.2017.12.003

45. Chen C, Miao W, Zhou C, Wu H (2017) Thermogravimetric pyrolysis kinetics of bamboo waste via Asymmetric Double Sigmoidal (Asym2sig) function deconvolution. Bioresour Technol 225:48–57. https://doi.org/10.1016/j.biortech.2016.11.013

46. Pinzi S, Buratti C, Bartocci P, Marseglia G, Fantozzi F, Barbanera M (2020) A simplified method for kinetic modeling of coffee silver skin pyrolysis by coupling pseudo-components peaks deconvolution analysis and model free- isoconversional methods. Fuel 278:118260. https://doi.org/10.1016/j.fuel.2020.118260

47. Sharma P, Pandey OP, Diwan PK (2019) Non-isothermal kinetics of pseudo-components of waste biomass. Fuel 253:1149–1161. https://doi.org/10.1016/j.fuel.2019.05.093

48. Müsellim E, Tahir MH, Ahmad MS, Ceylan S (2018) Thermokinetic and TG/DSC-FTIR study of pea waste biomass pyrolysis. Appl Therm Eng 137:54–61. https://doi.org/10.1016/j.applthermaleng.2018.03.050

49. Ahmad MS, Mehmood MA, Taqvi STH, Elkamel A, Liu CG, Xu J, Rahimuddin SA, Gull M (2017) Pyrolysis, kinetics analysis, thermodynamics parameters and reaction mechanism of Typha latifolia to evaluate its bioenergy potential. Bioresour Technol 245:491–501. https://doi.org/10.1016/j.biortech.2017.08.162

50. Alhumade H, da Silva JCG, Ahmad MS, Çakman G, Yıldız A, Ceylan S, Elkamel A (2019) Investigation of pyrolysis kinetics and thermal behavior of Invasive Reed Canary (Phalaris arundinacea)for bioenergy potential. J Anal Appl Pyrolysis 140:385–392. https://doi.org/10.1016/j.jaap.2019.04.018

51. Konwar K, Nath HP, Bhuyan N, Saikia BK, Borah RC, Kalita AC, Saikia N (2019) Effect of biomass addition on the devolatilization kinetics, mechanisms and thermodynamics of a northeast Indian low rank sub-bituminous coal. Fuel 256:115926. https://doi.org/10.1016/j.fuel.2019.115926

52. Ming X, Xu F, Jiang Y, Zong P, Wang B, Li J, Qiao Y, Tian Y (2020) Thermal degradation of food waste by TG-FTIR and Py-GC/MS: pyrolysis behaviors, products, kinetic and thermodynamic analysis. J Clean Prod 244:118713. https://doi.org/10.1016/j.jclepro.2019.118713

53. Vyazovkin S, Burnham AK, Favergeon L, Koga N, Moukhina E, Pérez-Maqueda LA, Sbirrazzuoli N (2020) ICTAC Kinetics Committee recommendations for analysis of multi-step kinetics. Thermochim Acta 689:178597. https://doi.org/10.1016/j.tca.2020.178597

54. Wang S, Dai G, Yang H, Luo Z (2017) Lignocellulosic biomass pyrolysis mechanism: a state-of-the-art review. Prog Energy Combust Sci 62:33–86. https://doi.org/10.1016/j.pecs.2017.05.004

55. Gao N, Li A, Quan C, du L, Duan Y (2013) TG-FTIR and Py-GC/MS analysis on pyrolysis and combustion of pine sawdust. J Anal Appl Pyrolysis 100:26–32. https://doi.org/10.1016/j.jaap.2012.11.009

56. Fournel S, Marcos B, Godbout S, Heitz M (2015) Predicting gaseous emissions from small-scale combustion of agricultural biomass fuels. Bioresour Technol 179:165–172. https://doi.org/10.1016/j.biortech.2014.11.100

57. Tahir MH, Çakman G, Goldfarb JL, Topcu Y, Naqvi SR, Ceylan S (2019) Demonstrating the suitability of canola residue biomass to biofuel conversion via pyrolysis through reaction kinetics, thermodynamics and evolved gas analyses. Bioresour Technol 279:67–73. https://doi.org/10.1016/j.biortech.2019.01.106

58. Daugaard DE, Brown RC (2003) Enthalpy for pyrolysis for several types of biomass. Energy and Fuels 17:934–939. https://doi.org/10.1021/ef020260x

Publisher's note Springer Nature remains neutral with regard to jurisdictional claims in published maps and institutional affiliations.